

Rare decay $H^+ \rightarrow W^+ \gamma$ in the minimal supersymmetric standard model

Sreerup Raychaudhuri* and Amitava Raychaudhuri

Department of Physics, University of Calcutta, 92 Acharya Prafulla Chandra Road, Calcutta-700 009, India

(Received 20 May 1993)

The amplitude for the one-loop-induced decay $H^+ \rightarrow W^+ \gamma$ is calculated in the 't Hooft–Feynman gauge in the minimal supersymmetric standard model concentrating on the scalar sector only. It is shown that Feynman graphs with gauge bosons, physical and unphysical scalars, and Faddeev-Popov ghosts in the loops undergo large cancellations to contribute negligibly to the final amplitude. The dominant contribution comes from graphs with internal t and b quarks. A numerical evaluation shows that if the charged Higgs boson is lighter than the t quark, then the branching ratio for this process can be as large as $\sim 7 \times 10^{-3}$. For a wide range of parameters, this could remain well within the range of detectability at the CERN LHC and SSC.

PACS number(s): 13.40.Hq, 12.10.Dm, 12.60.Jv, 14.80.Cp

I. INTRODUCTION

Despite the lack of success of recent attempts at Z^0 factories and the Fermilab Tevatron collider to find signals of new physics beyond the standard model (SM), physicists have not given up hope of finding such evidences. The reason for this is that the SM, as it now stands, is a patchwork of theoretical and phenomenological input, lacking credibility as an ultimate theory of the fundamental interactions. Apart from this, an important ingredient of the theory, the scalar Higgs boson, has not yet been found, though one hopes that the more powerful colliders of the future will be able to hit upon it. Attempts to go beyond the SM have been part of the lore of particle physics ever since the 1970s and many alternative models have been proposed to make up for its various inadequacies. A common feature of most of these models has been the introduction of extra gauge symmetries in the Lagrangian, discrete as well as continuous, and the introduction of complicated scalar structures to break these symmetries spontaneously. Consequently, when the Higgs mechanism operates in these extended models, one is often left with whole families of physical Higgs bosons which can lead to quite unexpected phenomenological consequences.

Perhaps the simplest extension of the SM with extra Higgs bosons is the one with two scalar doublets, originally proposed [1] to explain CP violation. This model, though inadequate for the purpose for which it was introduced, resurfaced in the 1980s as an integral part of many newer models, e.g., supersymmetric models [2], left-right symmetric models [3], etc. As supersymmetry continues to be one of the most attractive theoretical options when one goes beyond the SM, two scalar doublets have attracted considerable attention and a substantial literature has accrued [4] over the past decade.

A large portion of the phenomenological studies made

with two scalar doublets have been in the so-called minimal supersymmetric standard model (MSSM) where the number of free parameters in the scalar sector is restricted to just two, which can be chosen, without loss of generality, to be the mass of the charged scalar m_+ and $\tan\beta$, the ratio of the vacuum expectation values of the two doublets. Apart from the charged Higgs particle, the model predicts three neutral states: H^0 , h^0 (scalar), and A^0 (pseudoscalar). Evidence for these predictions has been looked for at the Z^0 factories and at the Fermilab Tevatron, thus far without success. Hopes are now being increasingly centered on the upcoming hadron colliders, the CERN Large Hadron Collider (LHC) and the Superconducting Super Collider (SSC), to produce and detect the Higgs bosons of the MSSM.

Arguably the most important new phenomenon arising in models with two scalar doublets (such as the MSSM) is the existence of elementary charged scalars, popularly called charged Higgs bosons. In the MSSM, the masses of the charged scalar, m_+ , and the neutral pseudoscalar, m_A , are related by the important sum rule

$$m_+^2 = m_W^2 + m_A^2, \quad (1)$$

which immediately tells us that $m_+ \geq m_W$. Thus, at an e^+e^- collider such as the CERN e^+e^- collider LEP II with $\sqrt{s} \simeq 2m_W$, charged Higgs pair production through $e^+e^- \rightarrow \gamma^* \rightarrow H^+H^-$ or $Z^{0*} \rightarrow H^+H^-$ will be kinematically suppressed if not disallowed. To produce these particles, then, one has to turn to a hadron collider reaching energies of the TeV scale. The Fermilab Tevatron proves inadequate because \sqrt{s} is not high enough to produce detectable numbers, but one expects the LHC and the SSC to produce charged Higgs particles copiously. At these machines, one has to distinguish between two distinct cases.

(i) $m_t < m_+ + m_b$: when the charged scalar H^+ is too heavy to be produced from the decay of a top quark. The dominant processes [5] leading to charged Higgs boson production are $g\bar{b} \rightarrow t\bar{H}^+$ and $t\bar{b} \rightarrow H^+$. Although one would expect these processes to be suppressed by the lower flux of t and b quarks coming from the proton com-

*Electronic address: srccrup@saha.ernet.in

pared to valence quarks, they are, nevertheless, rendered somewhat viable by the fact that the $\bar{t}bH^+$ vertex is enhanced by the factor $m_t/m_W \simeq 1.1-2.5$ (for $91 \text{ GeV} \leq m_t \leq 200 \text{ GeV}$) compared to the $\bar{u}dH^+$, $\bar{c}sH^+$ vertices.¹ (The competing Drell-Yan process $\bar{q}q \rightarrow \gamma^* \rightarrow H^+H^-$ and two-photon fusion $\gamma\gamma \rightarrow H^+H^-$ lead to production rates which are an order of magnitude smaller [6] and need not be considered further.) For example, with $m_t = m_+ = 200 \text{ GeV}$, it has been estimated [5] that, at the SSC with a luminosity of $10^4 \text{ pb}^{-1}\text{yr}^{-1}$, the above processes could lead to annual production of 10^6 charged Higgs bosons. At the LHC, the corresponding figure could be $\sim 7 \times 10^6$, which is an extrapolation from [5] assuming the production cross section varies as s and using the higher luminosity expected for LHC. These estimates correspond to $\tan\beta \sim 1$ and fall as $\tan\beta$ increases. For example, for $\tan\beta \sim 2$ the above values are suppressed by a factor of about 0.25. While these numbers are reasonably large, the dominant decay mode of the charged Higgs boson will be $H^+ \rightarrow \bar{t}b$ where the same factor m_t/m_W is responsible for enhancing the branching ratio. Thus, charged Higgs boson production at the SSC or LHC will be signaled by two or three hadronic jets, which could be completely swamped by the enormous QCD background at TeV energies [7]. Whether this will indeed be the case will depend on possibilities of judiciously applying kinematic cuts to suppress the backgrounds [8,9] and calls for further study. However, in order to detect the charged Higgs particle, a better option may be to look for some other decay mode with a cleaner signature which will make up for the lower event rate.

(ii) $m_t > m_+ + m_b$: when the charged scalar is light enough to be produced dominantly through top quark decay. The branching ratio for the decay $t \rightarrow H^+ b$ is a function of $\tan\beta$. For $\tan\beta = 2$, this branching ratio convoluted with the expected rate of $t\bar{t}$ production [10] can lead, for $m_t = 200 \text{ GeV}$ and $m_+ = 100 \text{ GeV}$, to $7(1.4) \times 10^7$ charged Higgs particles per year at the LHC (SSC) assuming a luminosity of $5 \times 10^5 (10^4) \text{ pb}^{-1}\text{yr}^{-1}$. We shall use these estimates as benchmark figures in the subsequent discussions. (Note, however, that for $\tan\beta = 6$, the rate of production would be a third of the above estimate. This is near the minimum of the $t \rightarrow H^+ b$ branching ratio as $\tan\beta$ varies.) The principal decay modes of the charged Higgs bosons, in this case, are $H^+ \rightarrow W^+ h^0$, $H^+ \rightarrow c\bar{s}$, $H^+ \rightarrow \tau^+ \nu_\tau$, all of which are plagued by large backgrounds. The best bet in this case might be to look for universality violations in the lepton spectrum [5,8,11]; but here, once again, it may be interesting to look for a rare decay mode with a small background. This may, in the long run, be easier to identify than the principal decay modes of the charged Higgs boson. It could also serve to clinch the issue of H^+ detection if an excess of heavy fermions is observed, since

universality violation could arise from other sources rather than a charged Higgs boson decay (such as mixing with a heavy vector doublet of fermions).

One of the most promising rare decay candidates is the process $H^+ \rightarrow W^+ \gamma$. Being a two-body decay this will produce a monoenergetic photon in the H^+ rest frame, so that one may hope for a peak in the electromagnetic spectrum corresponding to this energy. This photon may also be expected to be isolated from the direction of the W^+ unlike photons produced by bremsstrahlung. Unfortunately, there is no $W^+ H^- \gamma$ coupling at the tree level, so one requires to generate an effective coupling through quantum corrections at the one-loop level. In the 't Hooft-Feynman gauge, this calculation turns out to be a highly nontrivial exercise with more than 100 Feynman diagrams, including tadpoles (Fig. 1), contributing to the one-loop amplitude. In this work, we have made an exact calculation of the $W^+ H^- \gamma$ amplitude in the 't Hooft-Feynman gauge in the MSSM considering the scalar extension only. We have not included sparticle contributions through loops because these have been clearly shown [12] to be rather small. Our final result shows [13] that a branching ratio for this process as high as 7×10^{-5} can be achieved for some range of masses of the charged Higgs boson in the event of a heavy top quark in the mass range 150–200 GeV.² It should be possible to detect such a signal at the LHC or SSC where around 10^7 charged Higgs bosons could be produced every year. For a relatively light top quark in the range 91–150 GeV, less charged Higgs bosons are produced and the dominant $H^+ \rightarrow \bar{t}b$ decay mode drives the $H^+ \rightarrow W^+ \gamma$ branching ratio to $\sim 10^{-6}$ or less. Even then, detection of the $H^+ \rightarrow W^+ \gamma$ signal could be a distinct possibility at LHC, especially for the right range of parameters, viz., for $\tan\beta \leq 5.5$. Of course, for a proper study of these possibilities, one should consider the backgrounds and ways to eliminate them. A brief qualitative discussion of these is, therefore, called for.

The plan of this article is as follows. In Sec. II, the structure of the scalar sector is briefly discussed and the strategy of calculation laid out. Sections III and IV are devoted to the evaluation of contributions with bosonic and fermionic loops, respectively. Branching ratios for different choices of the unknown parameters are then elaborated in Sec. V and collider signatures and their possible backgrounds are briefly discussed in Sec. VI. Finally, our conclusions are described in Sec. VII. The Appendixes contain most of the detailed formulas which are not given in the text.

II. SCALAR MASSES AND COUPLINGS

We briefly describe the scalar sector of the minimal supersymmetric standard model [4], which is of relevance for this work. There are two scalar doublets, carrying

¹Recall that the couplings of u and d quarks to the charged Higgs bosons carry factors $m_{u,d}/m_W \leq 10^{-3}$ while the coupling of the $\bar{t}dH^+$ vertex is suppressed by the corresponding element of the Cabibbo-Kobayashi-Maskawa matrix.

²In Ref. [13], the branching ratio for $m_+ < (m_t + m_b)$ was overestimated by about an order of magnitude due to an error in our formula for the $H^+ \rightarrow \tau^+ \nu_\tau$ branching ratio. This has been corrected in the present work.

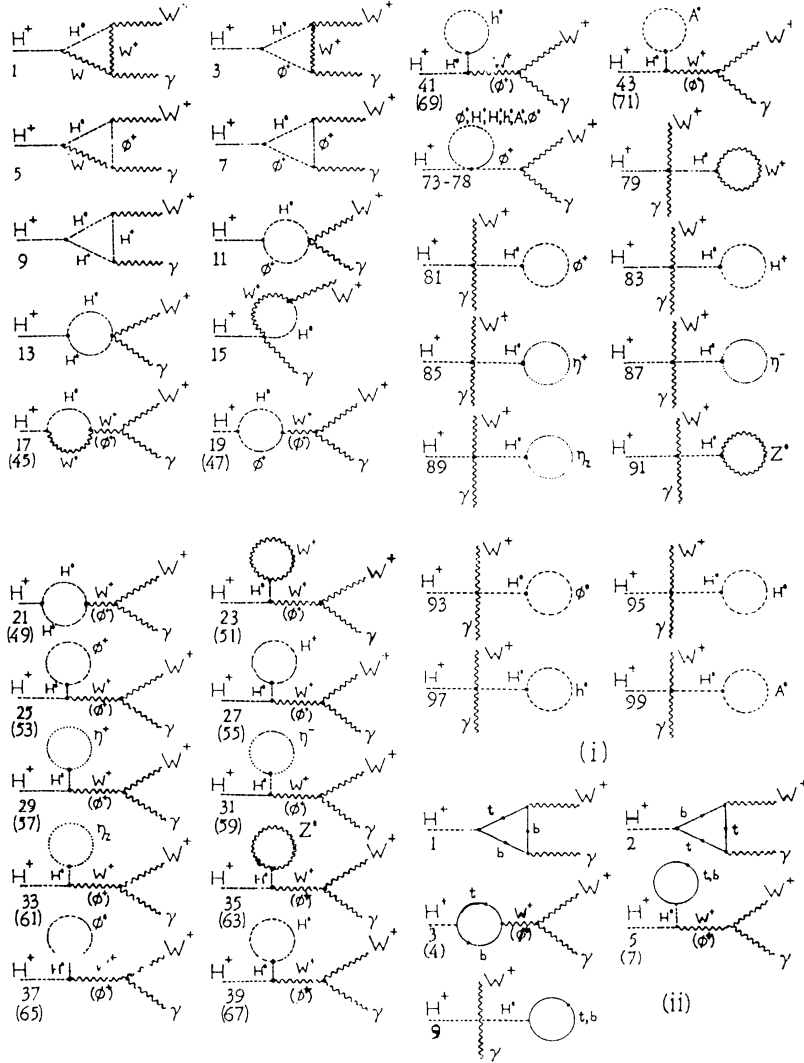


FIG. 1. Diagrams contributing to $H^+ \rightarrow W^+ \gamma$ with internal (i) bosonic and (ii) fermionic lines. Odd (even) numbered diagrams correspond to $H^0(h^0)$ propagators. Of these, only odd-numbered diagrams are shown.

hypercharge ± 1 :

$$\begin{aligned} \Phi_1^T &= [\phi_1^0 \ \phi_1^-], \\ \Phi_2^T &= [\phi_2^+ \ \phi_2^0]. \end{aligned} \quad (2)$$

The vacuum expectation values of these doublets are

$$\begin{aligned} \langle \Phi_1 \rangle^T &= [v_1 \ 0], \\ \langle \Phi_2 \rangle^T &= [0 \ v_2], \end{aligned} \quad (3)$$

where $v_1^2 + v_2^2 = v^2 = (\sqrt{2}G_F)^{-1}$. In terms of these doublets, the most general CP -invariant scalar potential obtained from a supersymmetric Lagrangian can be written in the form

$$\begin{aligned} V(\Phi_1, \Phi_2) &= m_1^2 \Phi_1^\dagger \Phi_1 + m_2^2 \Phi_2^\dagger \Phi_2 + m_{12}^2 (i \Phi_2^T \sigma_2 \Phi_1 + \text{H.c.}) \\ &+ \frac{g^2}{8 \cos^2 \theta_W} (\Phi_1^\dagger \Phi_1 - \Phi_2^\dagger \Phi_2)^2 + \frac{1}{2} g^2 |\Phi_1^\dagger \Phi_2|^2. \end{aligned} \quad (4)$$

After the electroweak symmetry is spontaneously bro-

ken, the physical scalar spectrum consists of (a) two charged Higgs bosons H^\pm , which are obtained from the equations

$$\begin{aligned} \phi_1^+ &= H^+ \sin \beta - \phi^+ \cos \beta, \\ \phi_2^+ &= H^+ \cos \beta + \phi^+ \sin \beta, \end{aligned} \quad (5)$$

where the ϕ^\pm are charged Goldstone bosons corresponding to the longitudinal modes of the W^\pm and $\tan \beta = v_1/v_2$, and (b) three neutral Higgs bosons H^0 , h^0 , and A^0 , of which the first two are CP even and the third is CP odd, given by the equations

$$\begin{aligned} \phi_1^0 &= v_1 + \frac{1}{\sqrt{2}} [(H^0 \cos \alpha - h^0 \sin \alpha) \\ &+ i(A^0 \sin \beta - \phi^0 \cos \beta)], \\ \phi_2^0 &= v_2 + \frac{1}{\sqrt{2}} [(H^0 \sin \alpha + h^0 \cos \alpha) \\ &+ i(A^0 \cos \beta + \phi^0 \sin \beta)], \end{aligned} \quad (6)$$

where the ϕ^0 is a neutral Goldstone boson corresponding

to the longitudinal mode of the Z^0 and α is the neutral Higgs mixing angle.

All the masses and couplings of these particles can be expressed in terms of the standard electroweak parameters with the introduction of just two new variables: viz., the mass m_+ of the charged Higgs boson and $\tan\beta$. The masses of the other scalars and the mixing angle α can be obtained from the formulas [14]

$$m_{H,h}^2 = \frac{1}{2} [m_Z^2 + m_A^2 \pm \sqrt{(m_Z^2 + m_A^2)^2 - 4m_Z^2 m_A^2 \cos^2 2\beta}], \quad (7)$$

$$\tan 2\alpha = \frac{m_A^2 + m_Z^2}{m_A^2 - m_Z^2} \tan 2\beta.$$

There are also two important relations involving the masses: viz., Eq. (1) and

$$m_H^2 + m_h^2 = m_Z^2 + m_A^2, \quad (8)$$

which are easily proved from the above, and which are required several times during the calculation of the $W^+ H^- \gamma$ coupling in the following sections. These identities, as well as complete Feynman rules for the above Higgs structure, may be found in Ref. [4].

The variation of the masses of the neutral scalars H^0 and h^0 with m_+ and $\tan\beta$ is shown in Figs. 2(i) and 2(ii), respectively. It may be noted that, as $m_+ \rightarrow \infty$, $m_H \rightarrow \infty$, $m_h \rightarrow m_Z |\cos 2\beta|$. m_H is rather less sensitive to variations in $\tan\beta$ than m_h . Taken in conjunction with the lower bound $m_h \geq 43$ GeV from LEP [15], it is clear that $\tan\beta = 1.5$ is ruled out at the tree level, but values of $\tan\beta \geq 2.5$ are allowed, especially for $m_+ \geq 100$ GeV—which, it will turn out, is the region of interest for the process studied in this paper.

The fact that there is no tree-level $W^+ H^- \gamma$ coupling in the MSSM is simply because the photon cannot connect two physical particles belonging to different irreducible representations of $U(1)_{em}$. This also shows up in the following argument based on electromagnetic gauge invariance of the amplitude [16]. The coupling must have the form $iM_{\mu\nu} \epsilon_W^\mu(p_1) \epsilon^\nu(p_2)$ where $M_{\mu\nu} = \lambda g m_W g_{\mu\nu}$ at the tree level, since it arises from the covariant derivative.

Gauge invariance demands that $p_2^\nu M_{\mu\nu} = 0$ implying $\lambda = 0$. At the one-loop level, however, $M_{\mu\nu}$ can have the general Lorentz structure

$$M_{\mu\nu} = \lambda \left[X g_{\mu\nu} + \frac{1}{m_Z^2} Y p_{1\nu} p_{2\mu} + \frac{1}{m_Z^2} Z \epsilon_{\mu\nu\alpha\beta} p_1^\alpha p_2^\beta \right], \quad (9)$$

taking into account transversality of the polarization vectors. The factor λ is included to make X, Y, Z dimensionless. Electromagnetic gauge invariance now merely demands that the form factors X, Y satisfy the identity

$$X + \frac{1}{m_Z^2} Y p_1 \cdot p_2 = 0. \quad (10)$$

The decay width for $H^+ \rightarrow W^+ \gamma$ can now be written in terms of the form factors as

$$\Gamma(H^+ \rightarrow W^+ \gamma) = \frac{\lambda^2}{64\pi m_+} \left[\frac{r_+ - r_W}{r_+} \right] |\bar{M}|^2, \quad (11)$$

where

$$|\bar{M}|^2 = 20|X|^2 + 8(r_+ - r_W) \text{Re}(X^* Y) + (r_+ - r_W)^2 (|Y|^2 + 2|Z|^2) \quad (12)$$

and $r_{+,W} = m_{+,W}^2/m_Z^2$. Although the parameters m_+ and $\tan\beta$ in this model are theoretically free to be chosen according to convenience, such a choice must be subject to experimental constraints. Chief among these is the lower bound [15] obtained from the LEP data on Z^0 decays. Clearly, as illustrated in Fig. 2(i), values of m_+ and $\tan\beta$ which lead to m_h inconsistent with this bound should be unacceptable. In using this constraint, however, there is a *caveat*. Recent work [17] on radiatively induced electroweak symmetry breaking in supersymmetric models with a heavy top quark has shown that the mass of the light neutral Higgs boson m_h receives large corrections which can push it up above the mass of the Z^0 boson. As a result, one gets an upper bound $m_h \leq 115$ GeV. Other masses such as m_H, m_A , etc. are largely unaffected. This could lead to significant changes in the way the above experimental constraint is imposed.

It has already been mentioned that the tree-level mass relations (1) and (8) play an important role in the calcula-

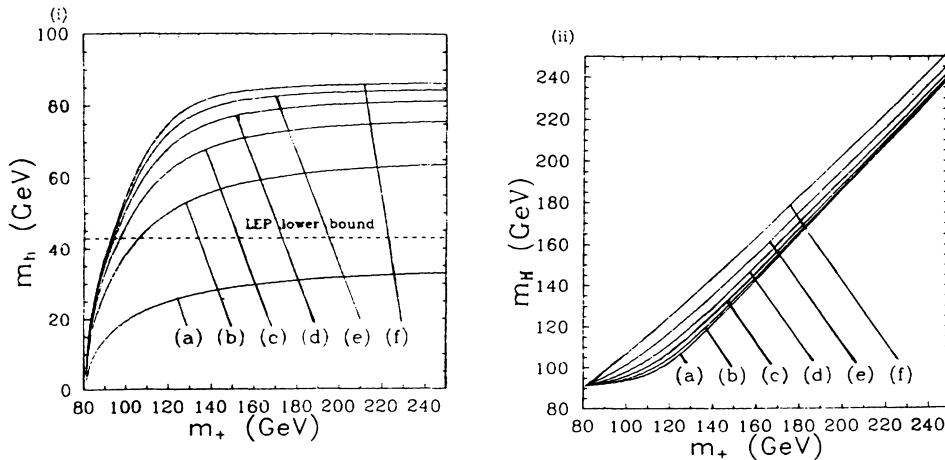


FIG. 2. Variation of the (i) light and (ii) heavy neutral scalar masses with m_+ for $\tan\beta =$ (a) 1.5, (b) 2.5, (c) 3.5, (d) 4.5, (e) 5.5, (f) 6.5. The broken line represents the experimental lower bound from LEP.

tion of the one-loop $W^+H^-\gamma$ amplitude. Incorporation of one-loop radiative corrections to the mass relations would necessitate the recalculation of the $W^+H^-\gamma$ amplitude at the *two-loop* level for consistency. It would be premature, at this stage, to consider such an approach when there is, as yet, no thorough understanding of this process at the one-loop level. In this work, therefore, we have used the *tree-level* mass relations only. As a result, we do not recommend that the constraint $\tan\beta > 2.5$ be taken too seriously in connection with this work.

In this context, it is also necessary to mention that we have not taken renormalized values of the masses and couplings. This is in accordance with the usual procedure for the calculation of one-loop generated processes which are absent at the tree level, since we expect the net amplitude to be finite in a renormalizable theory as it is not possible to have the corresponding counterterms. The price of not taking renormalized couplings is that we are forced to include the effects of all tadpole graphs in the final amplitude. We have chosen to work in the popular 't Hooft–Feynman gauge for a number of reasons. In this gauge, the Feynman rules can be checked against standard references, such as [18] and the very comprehensive appendixes of [4]. A more serious reason is the fact that the simple form of the gauge-boson propagator in this gauge turns out to be crucial for the numerical analysis of the problem. The alternative choice—to work in the unitary gauge where the number of diagrams to be evaluated is considerably less [19]—fails to compensate for a corresponding increase in the complexity of the calculation of each of those diagrams.³ Computation of these, keeping all internal and external masses, involves an enormous number of numerical steps leading to

a considerable loss of precision (due to round-off errors), as a result of which checks of finiteness and gauge invariance in this case could fail to work. With hindsight, we may further predict that the fine numerical cancellations between form factors obtained from different bosonic diagrams considered in our calculation may also get obscured by round-off errors in this situation. In the 't Hooft–Feynman gauge, however, the problem is avoided since we need to compute no more than tensors of rank two in the three-point functions.

III. $W^+H^-\gamma$ COUPLING WITH BOSONIC LOOPS

If one does not count fermions or sparticles, the $W^+H^-\gamma$ coupling can be generated at the one-loop level through a set of “bosonic” diagrams which are illustrated in Fig. 1(i). These diagrams, in the 't Hooft–Feynman gauge, can have massive gauge bosons W^\pm and Z^0 , physical scalars H^0 , h^0 , and A^0 , Goldstone bosons ϕ^\pm and ϕ^0 , and Faddeev-Popov ghosts η_\pm and η_Z in the internal lines. In Fig. 1(i), we have assigned odd (even) numbers to diagrams with H^0 (h^0) propagators and shown only the odd-numbered diagrams. The Feynman amplitude of each can now be written in terms of the one-, two-, and three-point functions defined in Appendix A. A full list is given in Appendix B. There are large cancellations among the different diagrams. The net amplitude, after all cancellations have taken place, can be written in the form of Eq. (9) with subscript b on λ , X , Y , and Z indicating that these are contributions from loops involving bosons only. These quantities are then given by

$$\lambda_b = \frac{-\alpha^{3/2}m_W}{4\sqrt{\pi}\sin^2\theta_W}\sin 2(\alpha-\beta),$$

$$X_b = \left\{ m_Z^2 r_A C_0(W, W, H) + \frac{r_W + r_+ - r_H}{2r_W} \left[2C_{24}(W, W, H) + \frac{r_W}{r_A} B_1(W, H; +) \right] \right. \\ \left. + \frac{r_H - 2r_W}{4r_W} \left[\frac{r_W}{r_A} \left[2B_1(+, H; +) + \frac{r_H - 2r_W}{r_W} [B_0(W, H; +) - B_0(+, H; +)] \right] + 4C_{24}(+, +, H) \right] \right. \\ \left. - \frac{r_+ + 3r_W}{4r_W} B_0(W, H; +) + B_0(W, H; W) - \frac{1}{4r_W} \left[A_H - \frac{r_H}{r_A} (A_+ - A_W) \right] \right\} - [H \leftrightarrow h], \quad (13)$$

$$\frac{1}{m_Z^2} Y_b = \left\{ 2C_0(W, W, H) - \frac{r_W + r_+ - r_H}{r_W} [C_{23}(W, W, H) - C_{22}(W, W, H)] \right. \\ \left. - \frac{r_H - 2r_W}{r_W} [C_{23}(+, +, H) - C_{22}(+, +, H)] \right\} - [H \leftrightarrow h], \quad (14)$$

$$\frac{1}{m_Z^2} Z_b = 0. \quad (15)$$

³To be precise, the $q_\mu q_\nu / M^2$ term arising in the gauge-boson propagator in the unitary gauge necessitates the inclusion of rank three and four tensors in the two- and three-point functions [20,21] constituting the amplitudes (see Appendixes).

The ratios r_i are defined by

$$r_i = m_i^2 / m_Z^2. \quad (16)$$

All C functions above have as arguments external masses $M_1 = m_W$, $M_2 = 0$, and $M_3 = m_+$. These have not been exhibited in the interests of brevity. The arguments i, j , and k shown correspond to the internal masses m_i, m_j , and m_k . Other notation and conventions used above are explained in Appendix B. An interesting feature of this amplitude is that it vanishes in the limit when the two particles H^0 and h^0 are mass degenerate. This is never the case in the MSSM (Fig. 2), but could be of interest in the context of a general two-Higgs-doublet model.

The above set of diagrams is both finite and gauge invariant. Finiteness is trivially checked following the prescriptions given in Appendix B. Checking gauge invariance is more complicated, as we need to verify Eq. (10) for this set of diagrams. Substituting the expanded forms of X_b and Y_b in the left-hand side of the above equation leads to a linear combination of one-, two-, and three-point functions which can then be written as a linear combination of the three basic functions A, B_0 , and C_0 using identities listed in Appendix A. After a straightforward, but tedious, calculation it turns out that the expressions

$$\Omega_b^i = X_b^i + \frac{1}{m_Z^2} Y_b^i p_1 \cdot p_2 \quad (i=1, 100) \quad (17)$$

can be written as linear combinations of the linearly independent functions

$$\begin{aligned} & C_0(W, W, H), \quad C_0(W, W, h), \quad C_0(+, +, H), \\ & C_0(+, +, h), \\ & B_0(W, W; \gamma), \quad B_0(W, H; W), \quad B_0(W, h; W), \\ & B_0(+, H; +), \quad B_0(+, h; +), \quad B_0(W, H; +), \\ & B_0(W, h; +), \\ & A(m_W), \quad A(m_+), \quad A(m_H), \quad A(m_h), \quad A(m_A), \\ & A(m_Z). \end{aligned} \quad (18)$$

While the individual Ω_b^i are nonvanishing, $\sum_{i=1}^{100} \Omega_b^i$ vanishes, with coefficients of each of the above functions canceling out separately. This, as it were, term-by-term can-

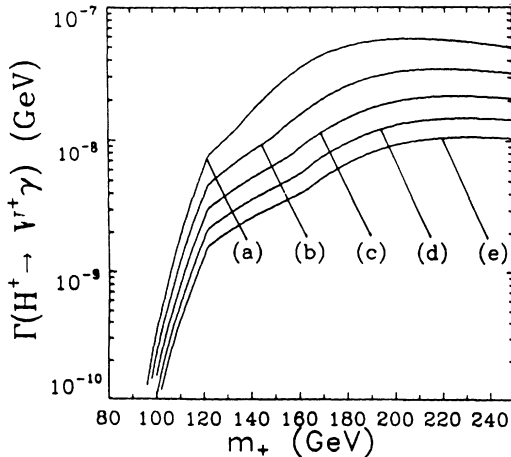


FIG. 3. Decay width for $H^+ \rightarrow W^+ \gamma$ with only bosonic loops for $\tan\beta =$ (a) 2.5, (b) 3.5, (c) 4.5, (d) 5.5, (e) 6.5.

cancellation happens to be an excellent check of the correctness of the final expression since trivial errors in the calculation of a single diagram would throw the corresponding cancellations out of gear. Once gauge invariance is established, finiteness, proved earlier, now follows quite

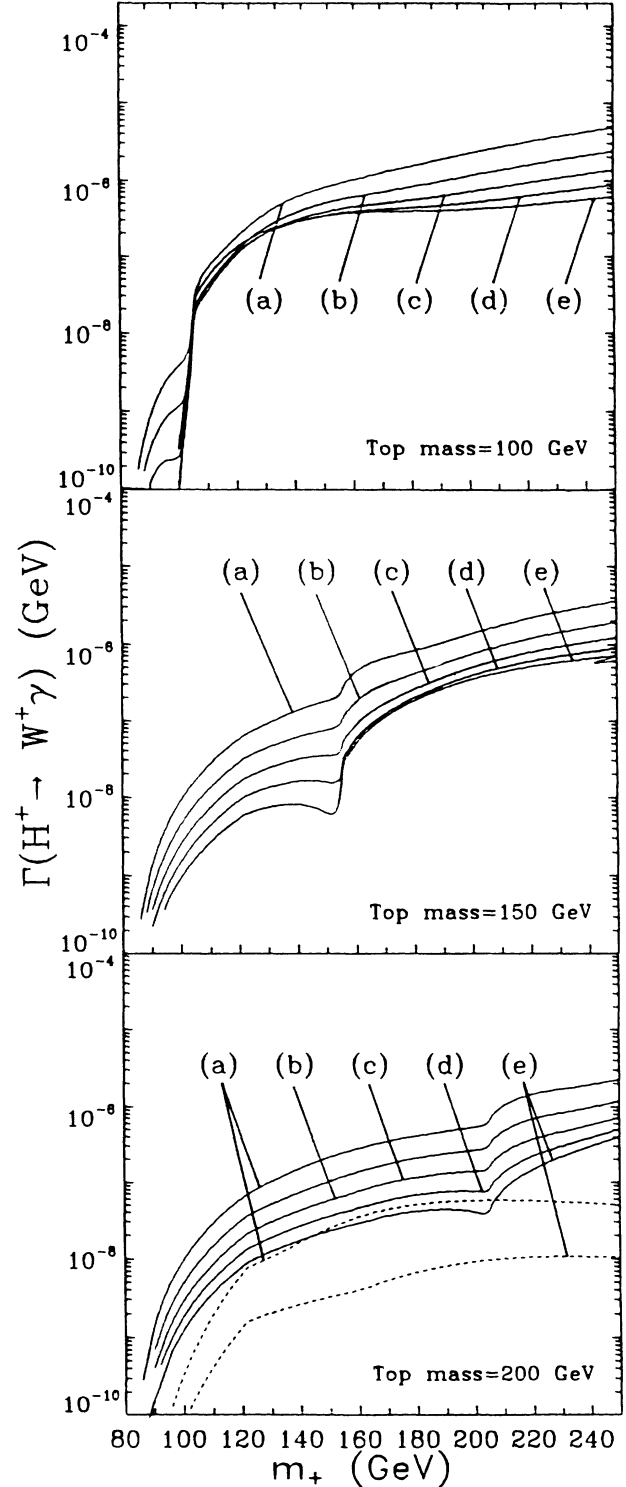


FIG. 4. Total decay width for $H^+ \rightarrow W^+ \gamma$ for $m_t =$ (i) 100 GeV, (ii) 150 GeV, and (iii) 200 GeV for $\tan\beta =$ (a) 2.5, (b) 3.5, (c) 4.5, (d) 5.5, (e) 6.5. In (iii), dotted lines show for comparison, the decay width with only bosonic loops.

easily. This is because the elements making up Y_b are finite by construction, so that the identity (10), written out in terms of divergent and finite parts, immediately tells us that $\text{div } X_b = \sum_i \text{div } X_i^b = 0$. The same argument also tells us that the linearly independent A , B , and C functions (18) which appear in the X_i 's, but not in the Y_i 's, will cancel out of the final X_b . This is the origin of the large cancellations which make the bosonic contributions so small.⁴

The form factors X_b , Y_b , and Z_b may be now plugged into Eq. (12) to obtain the decay width of $H^+ \rightarrow W^+ \gamma$ when only diagrams belonging to the above bosonic set are considered. In Fig. 3, we have shown this decay width for $H^+ \rightarrow W^+ \gamma$ as a function of m_+ and $\tan\beta$. We have considered values of $\tan\beta$ ranging from 2.5 to 6.5 and shown that the corresponding decay width does not exceed 6×10^{-8} , which is one to two orders of magnitude smaller than the contributions from top and bottom quark loops (see Fig. 4). For values of m_+ ranging between 80 and 120 GeV, the decay width is extremely small, mainly because of the limited phase space available. The decay width grows rapidly with m_+ and saturates around $m_+ = 150\text{--}200$ GeV for different values of $\tan\beta$. It may be noted that an increase in $\tan\beta$ leads to a fall in the width, though this variation is confined within an order of magnitude. We have also studied values of $\tan\beta > 6.5$ but these have not been shown in Fig. 3 as the decay width continues to show a steady fall as $\tan\beta$ continues to grow. Values of $\tan\beta \leq 1$ are uninteresting as they mimic the results for $\tan\beta \geq 1$. In any case, such values are disallowed in supersymmetric models where the electroweak symmetry is broken by radiative corrections to the scalar potential.

$$\lambda_f = -\alpha^{3/2} m_W / 2\sqrt{\pi} \sin^2 \theta_W ,$$

$$X_f = m_Z^2 \frac{r_A}{r_W} \left[R_t C_0(t, t, b) - \frac{R_b}{2} C_0(b, b, t) \right] + \frac{1}{2} S [8C_{24}(t, t, b) - 4C_{24}(b, b, t) - B_0(b, t; +)] \\ - \frac{3}{2} \frac{r_W}{r_A} \left[\left(\frac{2R_b}{r_W} + \frac{r_+}{r_W} D - \frac{S(D - S \cos 2\beta)}{\sin 2\beta} \right) B_0(b, t; +) + 2SB_1(b, t; +) - \frac{S}{r_W} (A_t - A_b) \right] + \frac{3}{2} DB_0(b, t; W) , \quad (19)$$

$$\frac{1}{m_Z^2} Y_f = -4S \{ [C_{23}(t, t, b) - C_{22}(t, t, b)] - \frac{1}{2} [C_{23}(b, b, t) - C_{22}(b, b, t)] \} + 2D [C_{12}(t, t, b) - \frac{1}{2} C_{12}(b, b, t)] \\ + \frac{1}{r_W} [2R_t C_0(t, t, b) - R_b C_0(b, b, t)] , \quad (20)$$

$$\frac{1}{m_Z^2} Z_f = \frac{1}{r_W} [2R_t C_0(t, t, b) + R_b C_0(b, b, t) + 2R_b C_{11}(b, b, t)] + 2SC_{12}(t, t, b) + DC_{12}(b, b, t) , \quad (21)$$

with all $r_i = m_i^2 / m_Z^2$ and $R_t = r_t \cot\beta$, $R_b = r_b \tan\beta$ while $S, D = (R_t \pm R_b) / r_W$. Other notation and conventions used above are explained in Appendix C. Once again, it can be shown, though not so trivially as in the bosonic case, that this amplitude vanishes in the limit when the

IV. $W^+ H^- \gamma$ COUPLING WITH FERMIONIC LOOPS

The $W^+ H^- \gamma$ coupling can also be generated at the one-loop level through a set of ‘‘fermionic’’ diagrams which are illustrated in Fig. 1(ii). These diagrams, in the 't Hooft–Feynman gauge, can have all generations of quarks in the internal lines. In Fig. 1(ii), we have again assigned odd (even) numbers to diagrams with H^0 (h^0) propagators and shown the odd-numbered ones only (apart from the cases where there are no H^0, h^0 propagators). For leptons, the diagram involving coupling of the photon to neutrinos is naturally absent. As before, the Feynman amplitude of each diagram can now be written in terms of the one-, two-, and three-point functions defined in Appendix A. A full list is given in Appendix C. It may be noted that the contributions due to leptons and quarks belonging to the first two generations are negligible due to their suppression by factors of m_f / m_W arising from the corresponding $H^+ \bar{f} f$ couplings. This same factor, as has been mentioned before, is responsible for an overwhelming dominance of diagrams with t and b quarks in the internal lines. Though some cancellations among the different diagrams do occur in this case also, it is not as dramatic as was the case with the ‘‘bosonic’’ diagrams, mainly because the $\epsilon_{\mu\nu\alpha\beta} p_1^\alpha p_2^\beta$ term is gauge invariant by construction, so that their coefficients Z_i are not constrained like the X_i and Y_i . The net amplitude with diagrams containing only t and b quarks, after all cancellations have taken place, can be written in the form of Eq. (9) with subscript f on λ , X , Y , and Z indicating that these are contributions from loops involving fermions only. These quantities are then given by

two particles H^0 and h^0 are mass degenerate.

This set of diagrams is separately finite and gauge invariant.⁵ As before, finiteness can be quite trivially checked following the prescriptions given in Appendix C.

⁴At this point it may be noted that the major contribution to $M_{\mu\nu}^b$ comes from X_b rather than Y_b which is small.

⁵We could, therefore, have calculated them in another gauge. For example, the authors of Ref. [12] have used the unitary gauge.

To check gauge invariance we need, once again, to verify Eq. (10) for this set of diagrams. As before, the expanded forms of X_f and Y_f in the left-hand side of the above equation can be written as a linear combination of the three basic functions A , B_0 , and C_0 using the identities listed in Appendix A. It is easy to check that the expressions

$$\Omega_f^i = X_f^i + \frac{1}{m_Z^2} Y_f^i p_1 \cdot p_2 \quad (i=1, 10) \quad (22)$$

can be written as linear combinations of the linearly independent functions

$$\begin{aligned} &C_0(t, t, b), \quad C_0(b, b, t), \\ &B_0(t, b; W), \quad B_0(t, b; +), \\ &A(m_t), \quad A(m_b). \end{aligned}$$

It is now possible to check that $\sum_{i=1}^{10} \Omega_f^i$ vanishes, coefficients of each of the above functions canceling out separately. Thus, we again have an excellent check of the correctness of the final expression. As Z_f is built up of finite functions only, finiteness of the net amplitude follows quite easily because, as in the bosonic case, the elements making up Y_f are finite by construction. The identity (10), written out in terms of divergent and finite parts immediately tells us that

$$\text{div } X_f = \sum_i \text{div } X_f^i = 0.$$

As before, linearly independent A , B , and C functions which occur in the X_i , but not in the Y_i , cancel out. This cancellation, naturally, does not apply to the Z_i .

Given the above expressions for the form factors X_f , Y_f , and Z_f , we are now in a position to calculate the *total* decay width for $H^+ \rightarrow W^+\gamma$ taking all diagrams into account. This can be done by using Eq. (12) with the overall factor

$$\lambda = -\alpha^{3/2} m_W / 2\sqrt{\pi} \sin^2 \theta_W$$

and

$$X = \frac{1}{2} \sin 2(\alpha - \beta) X_b + X_f \quad (23)$$

with similar equations for Y and Z , where, it may be recalled, $Z_b = 0$. In Figs. 4(i), 4(ii), and 4(iii) we have shown the variation in the $H^+ \rightarrow W^+\gamma$ decay width when contributions from *all* graphs have been taken into account, as a function of m_t and $\tan\beta$ for three different values of the top quark mass $m_t = 100, 150, \text{ and } 200$ GeV, respectively. Also shown with broken lines are corresponding contributions from bosonic loops only, illustrating the dominance of fermionic over bosonic contributions for the case $m_t = 200$ GeV. When the top quark mass is taken in the range 100–150 GeV, the bosonic contribution remains unchanged, but the fermionic contribution increases so that the dominance is even more marked. The curves shown have kinks near the $H^+ \rightarrow t\bar{b}$ threshold—a well-known numerical effect. As in the bosonic case, it may be seen that variations of $\tan\beta$ in the range 2.5–6.5 lead to no significant changes in the decay width beyond

a gradual fall within the same order of magnitude. The decay width remains small in the range $m_+ = 80\text{--}120$ GeV as in the purely bosonic case because of phase-space suppression and thereafter gradually saturates. It is interesting that the decay width falls very slightly as the top quark mass is increased from 100 to 200 GeV, though the net variation is rather small. This is because the enhancement resulting from the presence of couplings proportional to m_t is offset by suppression due to heavy top quark propagators. Similar behavior has been noticed [22] in the analogous cases of $H^0 \rightarrow \gamma\gamma$, $Z^0 \rightarrow H^0\gamma$, and $H^0 \rightarrow gg$, which occur in the SM.

Finally, we should note that for these last three processes, $H^0 \rightarrow \gamma\gamma$, $Z^0 \rightarrow H^0\gamma$, and especially $H^0 \rightarrow gg$, it has been shown [23] that the fermionic contributions are enhanced quite significantly by QCD corrections—though this does not change the total width for $H^0 \rightarrow \gamma\gamma$ and $Z^0 \rightarrow H^0\gamma$ much because these amplitudes are dominated by W loops. In the $H^+ \rightarrow W^+\gamma$ case, however, it is the *fermions* that dominate, which makes it analogous to the purely fermion-mediated case of $H^0 \rightarrow gg$. As a result, QCD corrections of the $H^+ \rightarrow W^+\gamma$ amplitude could have significant effects. This is a point which merits further study.

V. BRANCHING RATIOS FOR H^+ DECAY

In order to discuss branching ratios for the process $H^+ \rightarrow W^+\gamma$ it becomes necessary to consider the principal decay modes of the H^+ in the model in question. These are as follows.

(a) $H^+ \rightarrow \tau^+ \nu_\tau$. This channel is always open. The corresponding decay width is given by

$$\Gamma(H^+ \rightarrow \tau^+ \nu_\tau) = \frac{\alpha}{8 \sin^2 \theta_W} \frac{(m_+^2 - m_\tau^2)^2}{m_W^2 m_+^3} m_\tau^2 \tan^2 \beta. \quad (24)$$

(b) $H^+ \rightarrow c\bar{s}$. This channel is also open. The decay width is given by

$$\begin{aligned} \Gamma(H^+ \rightarrow c\bar{s}) = & \frac{3\alpha}{8 \sin^2 \theta_W} \frac{\sqrt{\lambda(m_+^2, m_c^2, m_s^2)}}{m_W^2 m_+^3} \\ & \times [(m_+^2 - m_c^2 - m_s^2)(m_c^2 \cot^2 \beta + m_s^2 \tan^2 \beta) \\ & - 4m_c^2 m_s^2], \end{aligned} \quad (25)$$

where

$$\lambda(a, b, c) = a^2 + b^2 + c^2 - 2ab - 2bc - 2ca.$$

It is important to note that both $H^+ \rightarrow \tau^+ \nu_\tau$ and $H^+ \rightarrow c\bar{s}$ have the same kinematic behavior as m_+ increases since, for all practical purposes, these fermions are massless compared to the H^+ which has mass $m_+ \geq m_W$. The only difference lies in the coupling ($m_c^2 \cot^2 \beta / m_W^2$) vs ($m_s^2 \tan^2 \beta / m_W^2$) and in the color factor for quarks.

As the mass of the charged Higgs boson increases, two other decay modes become kinematically accessible. These are the following.

(c) $H^+ \rightarrow W^+ h^0$: This channel opens for $m_+ \geq m_W + m_b$. The threshold is crossed for different

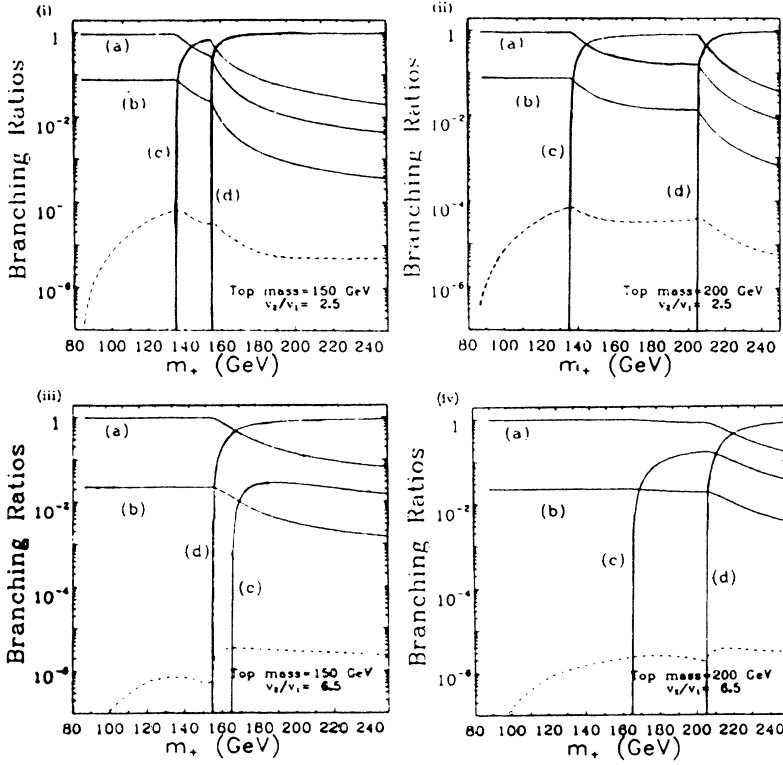


FIG. 5. Branching ratios of principal decay modes of the H^+ for (i) $m_t=150$ GeV and $\tan\beta=2.5$, (ii) $m_t=200$ GeV and $\tan\beta=2.5$, (iii) $m_t=150$ GeV and $\tan\beta=6.5$, (iv) $m_t=200$ GeV and $\tan\beta=6.5$. The solid lines correspond to (a) $H^+ \rightarrow \tau^+ \nu_\tau$, (b) $H^+ \rightarrow c\bar{s}$, (c) $H^+ \rightarrow W^+ h^0$, (d) $H^+ \rightarrow t\bar{b}$. The dotted line corresponds to $H^+ \rightarrow W^+ \gamma$ in each case.

values of m_+ depending on $\tan\beta$.⁶ The decay width is

$$\Gamma(H^+ \rightarrow W^+ h^0) = \frac{\alpha}{8 \sin^2 \theta_W} \frac{\lambda^{3/2}(m_+^2, m_W^2, m_h^2)}{2m_W^2 m_+^3} \cos^2(\beta - \alpha). \quad (26)$$

(d) $H^+ \rightarrow t\bar{b}$: This channel opens for $m_+ \geq m_t + m_b$. Hence, the threshold depends crucially on our choice of the mass of the top quark. The decay width is

$$\Gamma(H^+ \rightarrow t\bar{b}) = \frac{3\alpha}{8 \sin^2 \theta_W} \frac{\sqrt{\lambda(m_+^2, m_t^2, m_b^2)}}{m_W^2 m_+^3} \times [(m_+^2 - m_t^2 - m_b^2)(m_t^2 \cot^2 \beta + m_b^2 \tan^2 \beta) - 4m_t^2 m_b^2]. \quad (27)$$

This channel, when it is kinematically allowed, is the dominant decay mode of the charged Higgs boson.

These decay modes of the H^+ are illustrated in Figs. 5(i)–5(iv). It may be seen that for relatively small values of the charged Higgs boson mass, the $H^+ \rightarrow \tau^+ \nu_\tau$ mode dominates, followed by the $H^+ \rightarrow c\bar{s}$ mode. Broken lines show the behavior of the rare mode $H^+ \rightarrow W^+ \gamma$ which gradually rises as the phase-space factor increases. At some point, for small values of $\tan\beta$, the $H^+ \rightarrow W^+ h^0$ mode is excited, leading to a drop in all the other branching ratios. For this range of parameters, the

$H^+ \rightarrow W^+ h^0$ mode is the dominant one. For higher values of m_+ the $H^+ \rightarrow t\bar{b}$ mode becomes kinematically accessible and dominates all the others, leading to further drops in the corresponding branching ratios. The $t\bar{b}$ threshold depends on the mass of the top quark only and is independent of $\tan\beta$, but the $W^+ h^0$ threshold is pushed to higher values of m_+ as $\tan\beta$ increases. For example, for $\tan\beta=6.5$, in Fig. 5(iii) and 5(iv), this threshold is pushed beyond the $t\bar{b}$ threshold, so that it never becomes the dominant one. As a result, there are no significant changes in the $H^+ \rightarrow W^+ \gamma$ branching ratio when the corresponding threshold is crossed.

The detailed behavior of the branching ratio for $H^+ \rightarrow W^+ \gamma$ as a function of m_+ and $\tan\beta$ is shown for three values of the top quark mass in Figs. 6(i)–6(iii). It may be seen that the branching ratio rises sharply in the range $m_+ = 80$ –110 GeV because of the phase-space effect and thereafter tends to saturate. The branching ratio decreases as $\tan\beta$ increases from 2.5 to 6.5, though the variation remains confined within one to two orders of magnitude. Sudden drops in the branching ratio correspond to the crossing of thresholds for $H^+ \rightarrow W^+ h^0$ and $H^+ \rightarrow t\bar{b}$, as may be the case.⁷ For large values of m_+ the branching ratio remains steady at some value $\sim 10^{-5}$ – 10^{-6} . In Figs. 6(ii) and 6(iii), the variation of the $W^+ h^0$ threshold is well marked.

⁶Recall that $m_h = m_h(m_+, \tan\beta)$ in this model.

⁷Drops in the branching ratio for values of m_+ just before the threshold are a numerical artifact, as mentioned before. This erratic behavior becomes more prominent for $\tan\beta \geq 6.5$.

VI. COLLIDER SIGNATURES AND BACKGROUNDS

The possibility of observing this decay at the LHC or SSC will depend on the backgrounds and possible ways of eliminating them. As discussed in the Introduction, there

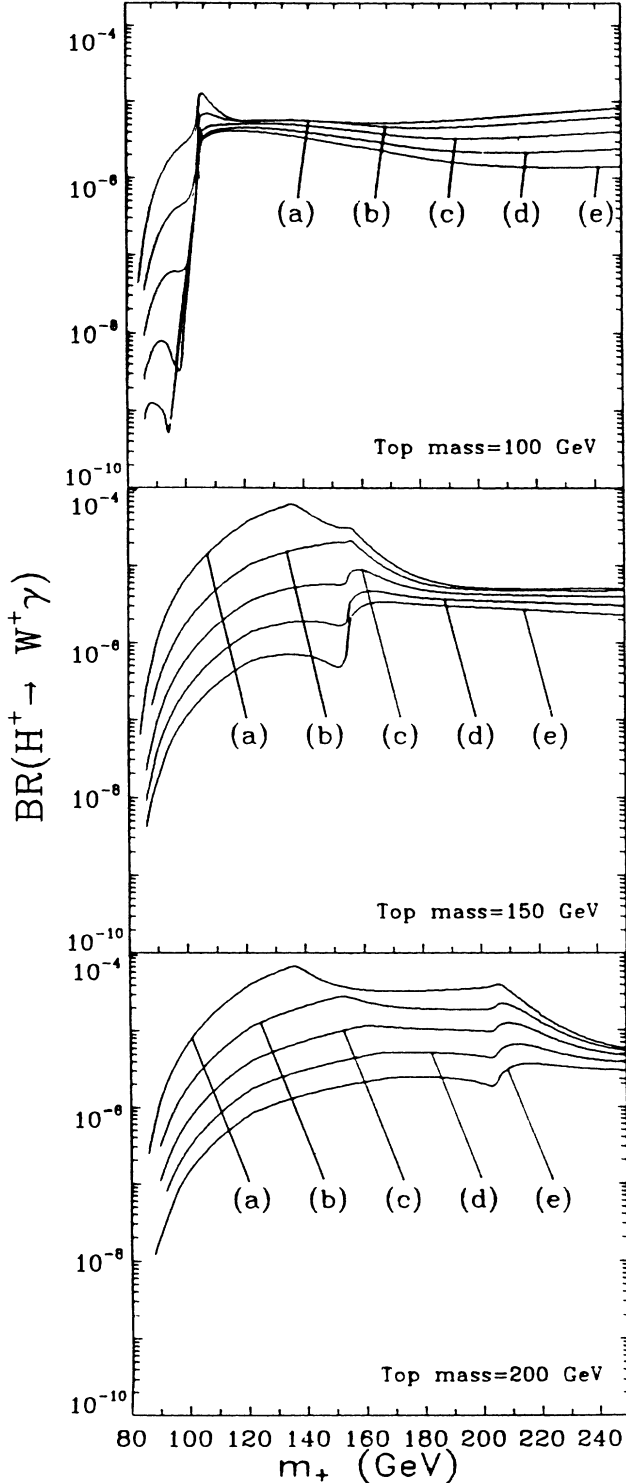


FIG. 6. Branching ratios for $H^+ \rightarrow W^+ \gamma$ for $m_t =$ (i) 100 GeV, (ii) 150 GeV, and (iii) 200 GeV for $\tan\beta =$ (a) 2.5, (b) 3.5, (c) 4.5, (d) 5.5, (e) 6.5.

are two distinct cases.

For $m_t < m_+ + m_b$, the hadronic production process will result in an H^+ and an associated \bar{t} (or an H^- and an associated t), which may be expected [7] to be moving nearly parallel to the original beam. The principal background will be a similar process [24] involving a W^+ and an associated \bar{t} (or a W^- and an associated t). The H^\pm can then decay to $W^\pm \gamma$. In the background process, this will be mimicked by a photon bremsstrahlung from the W^\pm or any of the other charged particles. Other backgrounds to the basic process $bg \rightarrow \bar{t}H^+$ can be removed almost completely [7] by triggering on a hard isolated lepton with $p_T > 10$ GeV. This has the effect of eliminating about 55% of the H^+ events also. It may be possible to eliminate the $bg \rightarrow \bar{t}W^{+\ast} \rightarrow \bar{t}W^+ \gamma$ events by applying a suitable isolation cut on the photon. We should also take into account the fact that the final W^\pm will itself decay into one or more charged particles and there could be a bremsstrahlung from any one of these lines. The forward-peaking of bremsstrahlung distributions will probably ensure that these cuts need not be very severe so far as the signal is concerned. For example, an angular cut of $20^\circ - 30^\circ$ should suppress most of the background where a photon is radiated from a W^\pm or its decay products. Finally the possibility of a t quark from the QCD sea radiating a H^0, h^0, A^0 which subsequently decays to two photons will have to be eliminated by ensuring that there is only *one* hard isolated photon. It might also be feasible to identify the W^+ (though not, perhaps, very accurately) from the jet-invariant mass when it decays hadronically. In summary, then, it does not seem unreasonable to assume that roughly 80% of the signal will be lost through various cuts. Assuming the remaining one-fifth to be detectable, in order to see *five* distinct events in a year's run, assuming benchmark figures for H^+ production as given in Sec. I, we require a minimum branching ratio:

$$B_{\min}(H^+ \rightarrow W^+ \gamma) = 3.5 \times 10^{-6} (2.5 \times 10^{-5})$$

at the LHC (SSC) for $\tan\beta = 2$.

The other case, $m_t > m_+ + m_b$, is more tricky. In this case we have a $t\bar{t}$ pair, one of which decays to a b -quark jet and an H^\pm . The H^\pm then decays to a W^\pm and a photon. As before, the identical process where the H^\pm is replaced by a W^\pm and there is a photon bremsstrahlung from any of the charged particle lines forms a serious background [24]. In this case we can no longer bank on the criterion that the final-state products will be moving along the beam jets. It will be necessary to trigger, as before, on a hard isolated lepton from the associated t or \bar{t} , but this alone will remove 80% of the events. A photon arising from an H^\pm decay will then have to be identified, as before, by its isolation from all charged particle tracks. Such a criterion should eliminate photons produced by bremsstrahlung from any of these charged particles. In addition, we have to ensure that there is only one isolated photon to avoid confusion with radiated neutral Higgs bosons which decay into two photons. Another possibility that may be taken into account for eliminating backgrounds without diminishing the signal drastically is the tagging of the b -quark jets arising from t decay. Some

criteria for this are discussed in Ref. [8]. It is also interesting that a b quark coming from $t \rightarrow bH^+$ is almost completely right handed. In view of the suggestion that charged Higgs bosons may be detectable from the polarization of τ 's in the decay $H^+ \rightarrow \tau^+ \nu_\tau$ (Bullock *et al.* in Ref. [11]), it might be useful to consider some way of identifying right-handed b jets. In the absence of a proper study, which certainly needs to be done,⁸ it may not be a bad estimate to assume that the various cuts remove 90% of the signal while eliminating all backgrounds almost completely. Assuming the remaining one-tenth to be detectable, one would require a minimum branching ratio

$$B_{\min}(H^+ \rightarrow W^+ \gamma) = 7.2 \times 10^{-7} (3.6 \times 10^{-6})$$

at the LHC (SSC). These benchmark figures should be multiplied by a factor of ~ 3 for $\tan\beta \simeq 6$ to take into account the dependence on $\tan\beta$ of the H^+ production process from t decay.

Prospects for observing this decay at the LHC or SSC may now be (crudely) estimated by comparing these minimum figures with the graphs shown in Figs. 6(i)–6(iii). There appears to be little hope of observing the decay at the SSC if $m_t < m_+ + m_b$ unless $m_t \simeq 200$ GeV and $\tan\beta \sim 2$. At the LHC, however, one could, perhaps, observe the decay for the entire range of top quark masses provided $\tan\beta \leq 5$. The situation may improve considerably for a light H^+ satisfying $m_t > m_+ + m_b$. In this case the decay is observable at the SSC for $\tan\beta \leq 3-4$ for almost the entire range of top quark masses except possibly for a small window near $m_t = 100$ GeV. For a light H^+ at the LHC, the decay should be observable for the whole range of parameter space studied.

VII. CONCLUSIONS

In this work, we have evaluated, in the minimal supersymmetric standard model, the decay width and branching ratio for the decay of a charged Higgs boson into a W boson and a monoenergetic photon in the H^+ rest frame—a rare decay mode which has good possibilities of detection at the upcoming pp colliders LHC and SSC. This is the first *complete* calculation of this process in any two-Higgs-doublet model in which the effects of a heavy top quark of mass 100–200 GeV have been analyzed in detail. The calculation is complete in the sense that the entire scalar sector contributions in the MSSM have been taken into account. In view of the fact that contributions to this process from graphs with sparticles in the internal

lines have been estimated to be rather small [12], this may be taken as a reasonable approximation to the complete $H^+ \rightarrow W^+ \gamma$ amplitude in the MSSM. Considered in the context of two-Higgs-doublet models, this particular one (the MSSM) is the most predictive since it has the smallest number of free parameters. For a more general two-Higgs-doublet model, the results may be different in the details, but we expect [25] the overall pattern to be somewhat similar. It is apparent from our results that, granted the problem of backgrounds can be handled, detection of this mode may prove a useful way to identify a charged Higgs boson at high-energy hadron colliders, and thereby establish the truth or otherwise of this model. The overwhelming dominance of t, b -quark loops in the MSSM, which has been proved in this work, is likely to be of help in the pursuance of further studies in this direction, since it renders computation of the decay width comparatively simple. Though more work, in particular, as regards backgrounds and QCD corrections, is obviously required, it appears that the $H^+ \rightarrow W^+ \gamma$ decay could assume a dominant role in charged Higgs boson detection at the upcoming supercolliders LHC and SSC.

ACKNOWLEDGMENTS

The authors wish to thank G. Bhattacharyya, A. Méndez, and S. D. Rindani for discussions. S.R. acknowledges financial support from the University Grants Commission, India. The research of A.R. was supported in part by the Department of Science and Technology, India and the Council of Scientific and Industrial Research, India.

APPENDIX A: LOOP INTEGRALS

The one-, two-, and three-point functions of 't Hooft and Veltman and Passarino and Veltman are defined below. All integrations are in Euclidean space.

One-point function:

$$A(m) \equiv \frac{1}{\pi^2} \int d^4q \frac{1}{q^2 + m^2}. \quad (\text{A1})$$

Scalar two-point function:

$$B_0(m_1, m_2; M) \equiv \frac{1}{\pi^2} \int d^4q \frac{1}{(q^2 + m_1^2)[(q+p)^2 + m_2^2]}, \quad (\text{A2})$$

where $p^2 = M^2$.

Scalar three-point function:

$$C_0(m_1, m_2, m_3; M_1, M_2, M_3) \equiv \frac{1}{\pi^2} \int d^4q \frac{1}{(q^2 + m_1^2)[(q+p_1)^2 + m_2^2][(q+p_1+p_2)^2 + m_3^2]}, \quad (\text{A3})$$

where $(p_1 + p_2)^2 = M_1^2$, $p_1^2 = M_2^2$, and $p_3^2 = M_3^2$.

⁸We hope this will be facilitated by our observation in this paper that t, b -quark loops are quite enough to estimate the $H^+ \rightarrow W^+ \gamma$ decay width.

Vector two-point function:

$$B_\mu(m_1, m_2; M) \equiv \frac{1}{\pi^2} \int d^4 q \frac{q_\mu}{(q^2 + m_1^2)[(q+p)^2 + m_2^2]} \\ \equiv p_\mu B_1(m_1, m_2; M). \quad (\text{A4})$$

Vector three-point functions [$C \equiv C_\mu(m_1, m_2, m_3; M_1, M_2, M_3)$]:

$$C_\mu \equiv \frac{1}{\pi^2} \int d^4 q \frac{q_\mu}{(q^2 + m_1^2)[(q+p_1)^2 + m_2^2][(q+p_1+p_2)^2 + m_3^2]} \\ \equiv p_{1\mu} C_{11} + p_{2\mu} C_{12}. \quad (\text{A5})$$

Tensor three-point functions:

$$C_{\mu\nu} \equiv \frac{1}{\pi^2} \int d^4 q \frac{q_\mu q_\nu}{(q^2 + m_1^2)[(q+p_1)^2 + m_2^2][(q+p_1+p_2)^2 + m_3^2]} \\ \equiv p_{1\mu} p_{1\nu} C_{21} + p_{2\mu} p_{2\nu} C_{22} + [p_{1\mu} p_{2\nu} + p_{2\mu} p_{1\nu}] C_{23} + \delta_{\mu\nu} C_{24}. \quad (\text{A6})$$

The form factors B_1 , C_{11} , C_{12} , C_{21} , C_{22} , C_{23} , and C_{24} can all be written [21] as linear combinations of the basic functions A , B_0 , and C_0 .

In order to prove gauge invariance of the amplitudes given in the text, we require the two identities

$$2B_1(m_1, m_2; M) + B_0(m_1, m_2; M) \\ = \frac{1}{M^2} [A(m_2) - A(m_1)] - \frac{m_1^2 - m_2^2}{M^2} B_0(m_1, m_2; M). \quad (\text{A7})$$

For

$$C_A = C_A(m_1, m_1, m_3, M_1, 0, M_3)$$

with $A = 22, 23, 24$,

$$4C_{24} + 4p_1 \cdot p_2 (C_{23} - C_{22}) \\ = \frac{1}{M_3^2} [A(m_3) - A(m_1)] \\ + (M_3^2 + m_3^2 - m_1^2) B_0(m_1, m_3; M_3). \quad (\text{A8})$$

These can be derived from the formulas given in Ref. [21] which express all form factors in terms of A , B_0 , and C_0 .

APPENDIX B: CONTRIBUTIONS FROM INDIVIDUAL DIAGRAMS WITH BOSONIC LOOPS

The $W^+ H^- \gamma$ coupling arising from the bosonic diagram numbered n [see Fig. 1(ii)] is given by Eq. (9) with $Z_b = 0$; i.e.,

$$M_{\mu\nu}^b = \frac{\alpha^{3/2} m_W}{4\sqrt{\pi} \sin^2 \theta_W} \sin 2(\alpha - \beta) \left[X_n^b \delta_{\mu\nu} + \frac{1}{m_Z^2} Y_n^b p_{1\nu} p_{2\mu} \right],$$

where the X_n^b and Y_n^b are listed below. It should be noted that $Y_n^b = 0$ for $n = 11 - 100$, so these have not been listed.

Some prior explanation of the notation used below is called for. All three-point functions have as common ar-

guments the external masses m_W , 0, and m_+ . These have been omitted for the sake of brevity. The C functions with internal masses m_i , m_j , and m_k have been denoted $C(i, j, k)$. For B functions, a similar convention has been adopted. We have denoted by $B(i, j; k)$ the two-point function with internal masses m_i and m_j and external mass m_k . For one-point functions, a slightly different notation has been used. We introduce the symbol A_i which is defined by

$$A_i = \frac{1}{m_Z^2} A(m_i),$$

while the symbols r_i are defined as in the text by the formulas $r_i = m_i^2 / m_Z^2$. The list of bosonic form factors is as follows:

$$X_1^b = \frac{1}{2}(r_+ + r_H - 2r_W) m_Z^2 C_0(W, W, H) + \frac{1}{2} C_{24}(W, W, H) \\ + \frac{1}{2} [B_0(W, H; W) - B_0(W, W; \gamma) - B_0(W, H; +)],$$

$$\frac{1}{m_Z^2} Y_1^b = -2C_0(W, W, H) - C_{11}(W, W, H) \\ - C_{12}(W, W, H) \\ - \frac{1}{2} C_{22}(W, W, H) + \frac{1}{2} C_{23}(W, W, H), \quad (\text{B1})$$

$$X_2^b = -\frac{1}{2}(r_+ + r_h - 2r_W) m_Z^2 C_0(W, W, h) \\ - \frac{1}{2} C_{24}(W, W, h) \\ - \frac{1}{2} [B_0(W, h; W) - B_0(W, W; \gamma) - B_0(W, h; +)],$$

$$\frac{1}{m_Z^2} Y_2^b = 2C_0(W, W, h) + C_{11}(W, W, h) + C_{12}(W, W, h) \\ + \frac{1}{2} C_{22}(W, W, h) - \frac{1}{2} C_{23}(W, W, h), \quad (\text{B2})$$

$$X_3^b = \frac{1}{2}(r_+ - r_H) m_Z^2 C_0(W, W, H), \\ \frac{1}{m_Z^2} Y_3^b = 0, \quad (\text{B3})$$

$$\begin{aligned} X_4^b &= -\frac{1}{2}(r_+ - r_h)m_Z^2 C_0(W, W, h), \\ \frac{1}{m_Z^2} Y_4^b &= 0, \end{aligned} \quad (\text{B4})$$

$$\begin{aligned} X_5^b &= \frac{1}{2}C_{24}(W, W, H), \\ \frac{1}{m_Z^2} Y_5^b &= C_{11}(W, W, H) - C_{12}(W, W, H) \\ &\quad - \frac{1}{2}C_{22}(W, W, H) + \frac{1}{2}C_{23}(W, W, H), \end{aligned} \quad (\text{B5})$$

$$\begin{aligned} X_6^b &= -\frac{1}{2}C_{24}(W, W, h), \\ \frac{1}{m_Z^2} Y_6^b &= -C_{11}(W, W, h) + C_{12}(W, W, h) \\ &\quad + \frac{1}{2}C_{22}(W, W, h) - \frac{1}{2}C_{23}(W, W, h), \end{aligned} \quad (\text{B6})$$

$$\begin{aligned} X_7^b &= \frac{r_+ - r_H}{r_W} C_{24}(W, W, H), \\ \frac{1}{m_Z^2} Y_7^b &= \frac{r_+ - r_H}{r_W} [C_{23}(W, W, H) - C_{22}(W, W, H)], \end{aligned} \quad (\text{B7})$$

$$\begin{aligned} X_8^b &= -\frac{r_+ - r_h}{r_W} C_{24}(W, W, h), \\ \frac{1}{m_Z^2} Y_8^b &= -\frac{r_+ - r_h}{r_W} [C_{23}(W, W, h) - C_{22}(W, W, h)], \end{aligned} \quad (\text{B8})$$

$$\begin{aligned} X_9^b &= \frac{r_H - 2r_W}{r_W} C_{24}(+, +, H), \\ \frac{1}{m_Z^2} Y_9^b &= \frac{r_H - 2r_W}{r_W} [C_{23}(+, +, H) - C_{22}(+, +, H)], \end{aligned} \quad (\text{B9})$$

$$\begin{aligned} X_{10}^b &= -\frac{r_h - 2r_W}{r_W} C_{24}(+, +, h), \\ \frac{1}{m_Z^2} Y_{10}^b &= -\frac{r_h - 2r_W}{r_W} [C_{23}(+, +, h) - C_{22}(+, +, h)], \end{aligned} \quad (\text{B10})$$

$$X_{11}^b = -\frac{r_+ - r_H}{4r_W} B_0(W, H; +), \quad (\text{B11})$$

$$X_{12}^b = \frac{r_+ - r_h}{4r_W} B_0(W, h; +), \quad (\text{B12})$$

$$X_{13}^b = -\frac{r_H - 2r_W}{4r_W} B_0(+, H; +), \quad (\text{B13})$$

$$X_{14}^b = \frac{r_h - 2r_W}{4r_W} B_0(+, h; +), \quad (\text{B14})$$

$$X_{15}^b = \frac{1}{2}B_0(W, H; W), \quad (\text{B15})$$

$$X_{16}^b = -\frac{1}{2}B_0(W, h; W), \quad (\text{B16})$$

$$X_{17}^b = \frac{r_W}{2r_A} [B_1(W, H; +) + 2B_0(W, H; +)], \quad (\text{B17})$$

$$X_{18}^b = -\frac{r_W}{2r_A} [B_1(W, h; +) + 2B_0(W, h; +)], \quad (\text{B18})$$

$$X_{19}^b = \frac{r_+ - r_H}{4r_A} [2B_1(W, H; +) + B_0(W, H; +)], \quad (\text{B19})$$

$$X_{20}^b = -\frac{r_+ - r_h}{4r_A} [2B_1(W, h; +) + B_0(W, h; +)], \quad (\text{B20})$$

$$X_{21}^b = \frac{r_H - 2r_W}{4r_A} [2B_1(+, H; +) + B_0(+, H; +)], \quad (\text{B21})$$

$$X_{22}^b = -\frac{r_h - 2r_W}{4r_A} [2B_1(+, h; +) + B_0(+, h; +)], \quad (\text{B22})$$

$$X_{23}^b = \frac{2r_W}{r_A r_H} A_W, \quad (\text{B23})$$

$$X_{24}^b = -\frac{2r_W}{r_A r_h} A_W, \quad (\text{B24})$$

$$X_{25}^b = \frac{1}{4r_A} A_W, \quad (\text{B25})$$

$$X_{26}^b = -\frac{1}{4r_A} A_W, \quad (\text{B26})$$

$$X_{27}^b = -\frac{r_H - 2r_W}{4r_H r_A} A_+, \quad (\text{B27})$$

$$X_{28}^b = \frac{r_h - 2r_W}{4r_h r_A} A_+, \quad (\text{B28})$$

$$X_{29}^b = -\frac{r_W}{4r_H r_A} A_W, \quad (\text{B29})$$

$$X_{30}^b = \frac{r_W}{4r_h r_A} A_W, \quad (\text{B30})$$

$$X_{31}^b = -\frac{r_W}{4r_H r_A} A_W, \quad (\text{B31})$$

$$X_{32}^b = \frac{r_W}{4r_h r_A} A_W, \quad (\text{B32})$$

$$X_{33}^b = -\frac{1}{8r_H r_A} A_Z, \quad (\text{B33})$$

$$X_{34}^b = \frac{1}{8r_h r_A} A_Z, \quad (\text{B34})$$

$$X_{35}^b = \frac{1}{r_H r_A} A_Z, \quad (\text{B35})$$

$$X_{36}^b = -\frac{1}{r_h r_A} A_Z, \quad (\text{B36})$$

$$X_{37}^b = \frac{1}{8r_A} A_Z, \quad (\text{B37})$$

$$X_{38}^b = -\frac{1}{8r_A} A_Z, \quad (\text{B38})$$

$$X_{39}^b = -\frac{3r_H + 3r_h - 6}{8r_A(r_H - r_h)} A_H, \quad (\text{B39})$$

$$X_{40}^b = \frac{3r_h^2 + 3r_H r_h - 2r_H - 4r_h}{8r_h r_A (r_H - r_h)} A_H, \quad (\text{B40})$$

$$X_{41}^b = \frac{3r_H^2 + 3r_H r_h - 2r_h - 4r_H}{8r_H r_A (r_H - r_h)} A_h, \quad (\text{B41})$$

$$X_{42}^b = -\frac{3r_H + 3r_h - 6}{8r_A (r_H - r_h)} A_h, \quad (\text{B42})$$

$$X_{43}^b = -\frac{1}{8r_A} A_A, \quad (\text{B43})$$

$$X_{44}^b = \frac{1}{8r_A} A_A, \quad (\text{B44})$$

$$X_{45}^b = \frac{1}{4r_A} [-A_H + 2A_W + (r_W - 2r_H - 2r_+) B_0(W, H; +)], \quad (\text{B45})$$

$$X_{46}^b = -\frac{1}{4r_A} [-A_h + 2A_W + (r_W - 2r_h - 2r_+) B_0(W, h; +)], \quad (\text{B46})$$

$$X_{47}^b = -\frac{r_H(r_+ - r_H)}{4r_W r_A} B_0(W, H; +), \quad (\text{B47})$$

$$X_{48}^b = \frac{r_h(r_+ - r_h)}{4r_W r_A} B_0(W, h; +), \quad (\text{B48})$$

$$X_{49}^b = \frac{(r_+ - r_H)(r_H - 2r_W)}{4r_W r_A} B_0(+, H; +), \quad (\text{B49})$$

$$X_{50}^b = -\frac{(r_+ - r_h)(r_h - 2r_W)}{4r_W r_A} B_0(+, h; +), \quad (\text{B50})$$

$$X_{51}^b = -\frac{2(r_+ - r_H)}{r_A r_H} A_W, \quad (\text{B51})$$

$$X_{52}^b = \frac{2(r_+ - r_h)}{r_A r_h} A_W, \quad (\text{B52})$$

$$X_{53}^b = -\frac{r_+ - r_H}{4r_W r_A} A_W, \quad (\text{B53})$$

$$X_{54}^b = \frac{r_+ - r_h}{4r_W r_A} A_W, \quad (\text{B54})$$

$$X_{55}^b = \frac{(r_+ - r_H)(r_H - 2r_W)}{4r_W r_H r_A} A_+, \quad (\text{B55})$$

$$X_{56}^b = -\frac{(r_+ - r_h)(r_h - 2r_W)}{4r_W r_h r_A} A_+, \quad (\text{B56})$$

$$X_{57}^b = \frac{r_+ - r_H}{4r_H r_A} A_W, \quad (\text{B57})$$

$$X_{58}^b = -\frac{r_+ - r_h}{4r_h r_A} A_W, \quad (\text{B58})$$

$$X_{59}^b = \frac{r_+ - r_H}{4r_H r_A} A_W, \quad (\text{B59})$$

$$X_{60}^b = -\frac{r_+ - r_h}{4r_h r_A} A_W, \quad (\text{B60})$$

$$X_{61}^b = \frac{r_+ - r_H}{8r_W r_H r_A} A_Z, \quad (\text{B61})$$

$$X_{62}^b = -\frac{r_+ - r_h}{8r_W r_h r_A} A_Z, \quad (\text{B62})$$

$$X_{63}^b = -\frac{r_+ - r_H}{r_W r_H r_A} A_Z, \quad (\text{B63})$$

$$X_{64}^b = \frac{r_+ - r_h}{r_W r_h r_A} A_Z, \quad (\text{B64})$$

$$X_{65}^b = -\frac{r_+ - r_H}{8r_W r_A} A_Z, \quad (\text{B65})$$

$$X_{66}^b = \frac{r_+ - r_h}{8r_W r_A} A_Z, \quad (\text{B66})$$

$$X_{67}^b = \frac{(r_+ - r_H)(3r_H + 3r_h - 6)}{8r_W r_A (r_H - r_h)} A_H, \quad (\text{B67})$$

$$X_{68}^b = -\frac{(r_+ - r_h)(3r_h^2 + 3r_H r_h - 2r_H - 4r_h)}{8r_W r_h r_A (r_H - r_h)} A_H, \quad (\text{B68})$$

$$X_{69}^b = -\frac{(r_+ - r_H)(3r_H^2 + 3r_H r_h - 2r_h - 4r_H)}{8r_W r_H r_A (r_H - r_h)} A_h, \quad (\text{B69})$$

$$X_{70}^b = \frac{(r_+ - r_h)(3r_H + 3r_h - 6)}{8r_W r_A (r_H - r_h)} A_h, \quad (\text{B70})$$

$$X_{71}^b = \frac{r_+ - r_H}{8r_W r_A} A_A, \quad (\text{B71})$$

$$X_{72}^b = -\frac{r_+ - r_h}{8r_W r_A} A_A, \quad (\text{B72})$$

$$X_{73}^b = -\frac{r_H - r_h}{2r_W r_A} A_W, \quad (\text{B73})$$

$$X_{74}^b = \frac{r_H - r_h}{2r_W r_A} A_+, \quad (\text{B74})$$

$$X_{75}^b = \frac{r_H + r_h + 2r_W - 2}{8r_W r_A} A_H, \quad (\text{B75})$$

$$X_{76}^b = -\frac{r_H + r_h + 2r_W - 2}{8r_W r_A} A_h, \quad (\text{B76})$$

$$X_{77}^b = \frac{r_H - r_h}{8r_W r_A} A_A, \quad (\text{B77})$$

$$X_{78}^b = -\frac{r_H - r_h}{8r_W r_A} A_Z, \quad (\text{B78})$$

$$X_{79}^b = \frac{2}{r_H} A_W, \quad (\text{B79})$$

$$X_{80}^b = -\frac{2}{r_h} A_W, \quad (\text{B80})$$

$$X_{81}^b = \frac{1}{4r_W} A_W, \quad (\text{B81})$$

$$X_{82}^b = -\frac{1}{4r_W} A_W, \quad (\text{B82})$$

$$X_{83}^b = -\frac{r_H - 2r_W}{4r_H r_W} A_+, \quad (\text{B83})$$

$$X_{84}^b = \frac{r_h - 2r_W}{4r_h r_W} A_+, \quad (\text{B84})$$

$$X_{85}^b = -\frac{1}{4r_H} A_W, \quad (\text{B85})$$

$$X_{86}^b = \frac{1}{4r_h} A_W, \quad (\text{B86})$$

$$X_{87}^b = -\frac{1}{4r_H} A_W, \quad (\text{B87})$$

$$X_{88}^b = \frac{1}{4r_h} A_W, \quad (\text{B88})$$

$$X_{89}^b = -\frac{1}{8r_H r_W} A_Z, \quad (\text{B89})$$

$$X_{90}^b = \frac{1}{8r_h r_W} A_Z, \quad (\text{B90})$$

$$X_{91}^b = \frac{1}{r_H r_W} A_Z, \quad (\text{B91})$$

$$X_{92}^b = -\frac{1}{r_h r_W} A_Z, \quad (\text{B92})$$

$$X_{93}^b = \frac{1}{8r_W} A_Z, \quad (\text{B93})$$

$$X_{94}^b = -\frac{1}{8r_W} A_Z, \quad (\text{B94})$$

$$X_{95}^b = -\frac{3r_H + 3r_h - 6}{8r_W(r_H - r_h)} A_H, \quad (\text{B95})$$

$$X_{96}^b = \frac{3r_h^2 + 3r_H r_h - 2r_H - 4r_h}{8r_h r_W(r_H - r_h)} A_H, \quad (\text{B96})$$

$$X_{97}^b = \frac{3r_H^2 + 3r_H r_h - 2r_h - 4r_H}{8r_H r_W(r_H - r_h)} A_h, \quad (\text{B97})$$

$$X_{98}^b = -\frac{3r_H + 3r_h - 6}{8r_W(r_H - r_h)} A_h, \quad (\text{B98})$$

$$X_{99}^b = -\frac{1}{8r_W} A_A, \quad (\text{B99})$$

$$X_{100}^b = \frac{1}{8r_W} A_A. \quad (\text{B100})$$

APPENDIX C: CONTRIBUTIONS FROM INDIVIDUAL DIAGRAMS WITH FERMIONIC LOOPS

As in the previous case, the $W^+ H^- \gamma$ coupling arising from the fermionic diagram numbered n [see Fig. 1(ii)] is given by Eq. (9): i.e.,

$$M_{\mu\nu}^f = \frac{\alpha^{3/2} m_W}{2\sqrt{\pi} \sin^2 \theta_W} \left[X_n^f \delta_{\mu\nu} + \frac{1}{m_Z^2} Y_n^f p_{1\nu} p_{2\mu} + \frac{1}{m_Z^2} Z_n^f \epsilon_{\mu\nu\alpha\beta} p_1^\alpha p_2^\beta \right],$$

where the X_n^f , Y_n^f , and Z_n^f are listed below. It should be noted that $Y_n^f = Z_n^f = 0$ for $n=3-10$, so these have not been listed.

It may be pointed out once more that only the diagrams and amplitudes with t and b quarks have been listed here. Contributions from other quark generations will follow exactly the same pattern if we ignore mixing between the generations. If we wish to include all generations with their mixings, it is only necessary to replace m_t and m_b everywhere by m_i^u, m_j^d and sum over all values $i, j=1, 2, 3$ of the generation indices after multiplying each diagram by the appropriate elements of the Cabibbo-Kobayashi-Maskawa matrix. For leptons, the picture is somewhat different because the diagram corresponding to no. 2 in Fig. 1(ii) is absent and the factors corresponding to x_b vanish. The rest is easily obtained. Inclusion of all these diagrams changes the result for only t and b quarks by considerably less than 1%. It should also be noted that since the charged Higgs boson couplings are proportional to the masses of the charge $\frac{2}{3}$ quarks, there is no Glashow-Iliopoulos-Maiani (GIM) cancellation.

The notation follows most of the conventions set up in Appendix B. We need to introduce two new symbols R_t and R_b which are defined by

$$R_t = r_t \cot \beta, \\ R_b = r_b \tan \beta,$$

and in terms of these we write $S, D = (R_t \pm R_b)/r_W$. The list of form factors follows:

$$X_1^f = -\frac{1}{4} \left[2 \frac{r_A R_b}{r_W} m_Z^2 C_0(b, b, t) + S[8C_{24}(b, b, t) - 2B_0(b, t; +)] - 2DB_0(b, t; W) \right], \\ \frac{1}{m_Z^2} Y_1^f = \frac{R_b}{r_W} C_0(b, b, t) - 2S[C_{23}(b, b, t) - C_{22}(b, b, t)] - DC_{12}(b, b, t), \\ \frac{1}{m_Z^2} Z_1^f = \frac{R_b}{r_W} C_0(b, b, t) + 2 \frac{R_b}{r_W} C_{11}(b, b, t) + DC_{12}(b, b, t), \quad (\text{C1}) \\ X_2^f = \frac{r_A R_t}{r_W} m_Z^2 C_0(t, t, b) + S[4C_{24}(t, t, b) - B_0(b, t; +)] + DB_0(b, t; W), \\ \frac{1}{m_Z^2} Y_2^f = -2 \frac{R_t}{r_W} C_0(t, t, b) + 4S[C_{23}(t, t, b) - C_{22}(t, t, b)] - 2DC_{12}(t, t, b),$$

$$\frac{1}{m_Z^2} Z_2^f = 2 \frac{R_t}{r_W} C_0(t, t, b) + S C_{12}(t, t, b), \quad (C2)$$

$$X_3^f = -\frac{3r_W}{r_A} \left[S B_1(b, t; +) + \frac{R_b}{r_W} B_0(b, t; +) \right], \quad (C3)$$

$$X_4^f = -\frac{3}{2r_A} \{ D [A_t + A_b + r_+ B_0(b, t; +)] - S \csc 2\beta (D - S \cos 2\beta) B_0(b, t; +) \}, \quad (C4)$$

$$X_5^f = -\frac{3r_W}{r_A r_H} \sin(\beta - \alpha) \times \left[\frac{R_t}{r_W} \sin \alpha \sec \beta A_t + \frac{R_b}{r_W} \cos \alpha \csc \beta A_b \right], \quad (C5)$$

$$X_6^f = \frac{3r_W}{r_A r_h} \cos(\beta - \alpha) \times \left[\frac{R_t}{r_W} \cos \alpha \sec \beta A_t - \frac{R_b}{r_W} \sin \alpha \csc \beta A_b \right], \quad (C6)$$

$$X_7^f = \frac{3(r_+ - r_H)}{r_A r_H} \sin(\beta - \alpha) \times \left[\frac{R_t}{r_W} \sin \alpha \sec \beta A_t + \frac{R_b}{r_W} \cos \alpha \csc \beta A_b \right], \quad (C7)$$

$$X_8^f = -\frac{3(r_+ - r_h)}{r_A r_h} \cos(\beta - \alpha) \times \left[\frac{R_t}{r_W} \cos \alpha \sec \beta A_t - \frac{R_b}{r_W} \sin \alpha \csc \beta A_b \right], \quad (C8)$$

$$X_9^f = -\frac{3}{r_H} \sin(\beta - \alpha) \times \left[\frac{R_t}{r_W} \sin \alpha \sec \beta A_t + \frac{R_b}{r_W} \cos \alpha \csc \beta A_b \right], \quad (C9)$$

$$X_{10}^f = \frac{3}{r_h} \cos(\beta - \alpha) \times \left[\frac{R_t}{r_W} \cos \alpha \sec \beta A_t - \frac{R_b}{r_W} \sin \alpha \csc \beta A_b \right]. \quad (C10)$$

Finiteness of the sum $\sum_i X_i^f$ is shown exactly as in the bosonic case, while the Y_n^f and Z_n^f are finite by construction.

-
- [1] T. D. Lee, Phys. Rep. **9C**, 143 (1973).
[2] For a review, see, for example, H. E. Haber and G. Kane, Phys. Rep. **117**, 75 (1985).
[3] J. C. Pati and A. Salam, Phys. Rev. D **10**, 275 (1974); R. N. Mohapatra and J. C. Pati, *ibid.* **11**, 566, 2556 (1975); G. Senjanović and R. N. Mohapatra, *ibid.* **12**, 1502 (1975).
[4] J. F. Gunion, H. E. Haber, G. L. Kane, and S. Dawson, *The Higgs Hunter's Guide* (Addison-Wesley, Reading, MA, 1990). This reference includes a comprehensive survey of the literature.
[5] J. F. Gunion, H. E. Haber, F. E. Paige, Wu-Ki Tung, and S. S. D. Willenbrock, Nucl. Phys. **B294**, 621 (1987); A. C. Bawa, C. S. Kim, and A. D. Martin, Z. Phys. C **47**, 75 (1990).
[6] S. K. Oh *et al.*, Z. Phys. C **46**, 267 (1990).
[7] See, for example, p. 228 of Ref. [4] and references therein.
[8] R. M. Barnett *et al.*, Phys. Rev. D **47**, 1048 (1993).
[9] D. P. Roy (private communication).
[10] *Proceedings of the ECFA Large Hadron Collider Workshop*, Aachen, Germany, 1990, edited by G. Jarlskog and D. Rein (CERN Report No. 90-10, Geneva, Switzerland, 1990); C. H. Llewellyn Smith (private communication).
[11] I. Bigi *et al.*, Phys. Lett. B **181**, 157 (1986); V. Barger and R. J. N. Phillips, Phys. Rev. D **41**, 884 (1990); R. M. Godbole and D. P. Roy, *ibid.* **43**, 3640 (1991); M. Drees and D. P. Roy, Phys. Lett. B **269**, 155 (1991); B. K. Bullock, K. Hagiwara, and A. D. Martin, Phys. Rev. Lett. **67**, 3055 (1991); D. P. Roy, Phys. Lett. B **283**, 403 (1992).
[12] M. Capdequi-Peyranère, H. E. Haber, and P. Irulegui, Phys. Rev. D **44**, 191 (1991).
[13] S. Raychaudhuri and A. Raychaudhuri, Phys. Lett. B **297**, 159 (1992).
[14] J. F. Gunion and H. E. Haber, Nucl. Phys. **B278**, 449 (1986).
[15] L3 Collaboration, B. Adeva *et al.*, Phys. Lett. B **283**, 454 (1992).
[16] J. A. Grifols and A. Méndez, Phys. Rev. D **22**, 1725 (1980); A. A. Iogansen, N. G. Uraltsev, and V. A. Khoze, Yad. Fiz. **36**, 1230 (1982) [Sov. J. Nucl. Phys. **36**, 717 (1982)]; A. Méndez and A. Pomarol, Nucl. Phys. **B349**, 369 (1991).
[17] J. F. Gunion and J. Türski, Phys. Rev. D **39**, 2701 (1989); **40**, 2333 (1989); **40**, 2325 (1989); E. Berger, *ibid.* **41**, 225 (1990); Y. Okada, H. Yamaguchi, and T. Yanagida, Prog. Theor. Phys. Lett. B **5**, 1 (1991); Phys. Lett. B **262**, 54 (1991); J. Ellis, G. Ridolfi, and F. Zwirner, *ibid.* **257**, 81 (1991); **262**, 477 (1991); H. E. Haber and R. Hempfling, Phys. Rev. Lett. **66**, 1815 (1991); R. Barbieri, M. Frigeni, and F. Caravaglios, Phys. Lett. B **258**, 167 (1991); R. Barbieri and M. Frigeni, *ibid.* **256**, 395 (1991); A. Yamada, *ibid.* **263**, 233 (1991); P. Chankowski, IFT Report No. 91-7-Warsaw (unpublished).
[18] D. Bailin and A. E. Love, *Introduction to Gauge Field Theories* (Hilger, London, 1986).
[19] J. F. Gunion, G. L. Kane, and J. Wudka, Nucl. Phys. **B299**, 231 (1988).
[20] G. 't Hooft and M. Veltman, Nucl. Phys. **B153**, 365 (1979).
[21] G. Passarino and M. Veltman, Nucl. Phys. **B160**, 151 (1979).
[22] R. N. Cahn, M. S. Chanowitz, and N. Fleishon, Phys. Lett. **82B**, 113 (1979); L. Bergstrom and G. Hulth, Nucl. Phys. **B259**, 137 (1985).
[23] A. Djouadi *et al.*, Phys. Lett. B **257**, 187 (1991); M. Spira *et al.*, *ibid.* **276**, 350 (1991); P. Zerwas *et al.*, *ibid.* **264**, 440 (1991).
[24] This is clear from the diagram on p. 218 of Ref. [4] for $\tan \beta > 1$.
[25] S. Raychaudhuri (unpublished).